Resonant Kelvin-Helmholtz modes in sheared relativistic flows

Manuel Perucho,[1,2,*] Michal Hanasz,[3] José-María Martí,[1] and Juan-Antonio Miralles[4]
[1]*Departament d'Astronomia i Astrofísica, Universitat de València, València, Spain*
[2]*Max-Planck-Institut für Radioastronomie, Bonn, Germany*
[3]*Toruń Centre for Astronomy, Nicholas Copernicus University, Toruń, Poland*
[4]*Departament de Física Aplicada, Universitat d'Alacant, Alacant, Spain*
(Received 20 September 2006; published 25 May 2007)

Certain aspects of the (linear and nonlinear) stability of sheared relativistic (slab) jets are analyzed. The linear problem has been solved for a wide range of jet models well inside the ultrarelativistic domain (flow Lorentz factors up to 20, specific internal energies $\approx 60c^2$). As a distinct feature of our work, we have combined the analytical linear approach with high-resolution relativistic hydrodynamical simulations, which has allowed us (i) to identify, in the linear regime, resonant modes specific to the relativistic shear layer, (ii) to confirm the result of the linear analysis with numerical simulations, and (iii) more interestingly, to follow the instability development through the nonlinear regime. We find that very-high-order reflection modes with dominant growth rates can modify the global, long-term stability of the relativistic flow. We discuss the dependence of these resonant modes on the jet flow Lorentz factor and specific internal energy and on the shear-layer thickness. The results could have potential applications in the field of extragalactic relativistic jets.

DOI: 10.1103/PhysRevE.75.056312 PACS number(s): 47.20.Ft, 47.75.+f, 98.58.Fd

I. INTRODUCTION

The Kelvin-Helmholtz (KH) instability (in the simplest case, that of a tangential discontinuity of velocity at the interface of parallel flows) is one of the classical instabilities in fluid dynamics. Linear perturbation analysis of KH instability has been presented for many situations including incompressible and compressible fluids, surface tension, finite shear layers, and magnetized fluids [1].

The linear analysis of the KH instability for fluids in relativistic relative motion (infinite, single-vortex-sheet approximation) was developed in the 1970s in the context of the stability of jets in extended extragalactic radio sources [2]. The main conclusion of these studies was the reduction of the maximum growth rate for increasing relative Lorentz factor flows and decreasing specific internal energies (or sound speeds). The general dispersion relation for relativistic cylindrical jets was obtained and solved for a range of parameter combinations of astrophysical interest [3,4]. Some approximate analytical expressions were derived [5]. General numerical solutions of the dispersion relation were analyzed [6] and the results were applied for the first time to the interpretation of the morphology of jets in extended radio sources and the motion of radio components in the inner part of these objects. Stability analysis (both in nonrelativistic and relativistic regimes) at KH instability has been used to interpret many phenomena observed in astrophysical jets such as quasiperiodic wiggles and knots, filaments, limb brightening, and jet disruption [7,8]. More recently, KH linear stability analysis applied to very-high-resolution observations was used to probe the physical parameters in these sources [9].

A general treatment of the KH instability with compressible shear layers in the case of infinite plane boundary (nonrelativistic) problems was proposed [10]. The study of the effects of shear layers was extended to the case of infinite slab jets [11], concentrating on the wave number range $0.1/R_j \leqslant k \leqslant 10/R_j$ (R_j is the jet radius) for ordinary ($n_x=0$) and the first-reflection ($n_x=1,2,3$) symmetric and antisymmetric modes (n_x represents the number of nodes across the planar jet).

An attempt to investigate the growth of the KH instability in some particular class of cylindrical relativistic sheared jets was pursued [12]. However, it was limited to the ordinary ($n_r=0$) and first two reflection modes ($n_r=1,2$), and the domain of jet parameters considered involved only marginally relativistic flows (beam flow velocities $\leqslant 0.1c$, where c is the speed of light) and nonrelativistic (jet, ambient) sound speeds ($\leqslant 0.01c$). Other approaches to the linear analysis of the stability of relativistic stratified jets [13] and sheared, ultrarelativistic jets [14] have also been performed. In the latter reference, the author has derived approximated formulas for instability modes excited in the shear layer.

In this paper, we report on certain aspects of the stability of sheared relativistic (slab) jets in linear and nonlinear regimes. We have considered a wide range of jet and ambient parameters reaching well inside the ultrarelativistic domain (jet flow Lorentz factors up to 20, jet specific internal energies $\approx 60c^2$). Instead of focusing on the stabilization effect of the shear layer on the ordinary modes alone [12], we have also studied the properties of very-high-order ($n_x \gtrsim 20$) reflection modes which have the largest growth rates and then dominate the global stability properties of the flow. Finally, we have combined the analytical linear approach with high-resolution relativistic hydrodynamical simulations which have allowed us (i) to confirm the results obtained with the linear analysis and (ii) to follow the instability development through the nonlinear regime. Our selection of the two-dimensional slab geometry for our work responds to several reasons: (i) the possibility of using larger resolutions in two-dimensional simulations, compared to fully three-dimensional simulations, (ii) the fact that slab jets allow for

*Electronic address: perucho@mpifr-bonn.mpg.de

the study of symmetric and antisymmetric modes, contrary to cylindric geometry, which only allows for symmetric structures, (iii) it is easier to solve the linear problem equation and to interpret results from the numerical simulations in this case, so we can gain deep knowledge of the physics of instabilities before studying more complex (including three dimensions, magnetic fields, etc.) problems. Several recent works have combined linear analysis and hydrodynamical simulations in connection with several astrophysical scenarios (i.e., relativistic jets [15] and *γ-ray bursts* [16]), the relativistic nature of the jet parameters considered (that includes the ultrarelativistic limit), the modes explored (very-high-order reflection modes), and the complementarity of linear analysis and nonlinear high-resolution simulations make the present work unique. The results of the numerical simulations in the nonlinear regime are presented elsewhere [17]. The results shown in this paper concerning the stability of relativistic sheared flows could be of potential interest in the field of extragalactic relativistic jets.

II. INSTABILITIES IN SHEARED RELATIVISTIC JETS: LINEAR ANALYSIS

We start with the equations governing the evolution of a slab relativistic perfect-fluid jet for which the energy-momentum tensor can be written as

$$T^{\mu\nu} = (\rho_e + P)u^\mu u^\nu + P\eta^{\mu\nu} \tag{1}$$

(units have been used so that $c=1$; Greek indices μ and ν run from 0 to 3), where ρ_e is the energy density, P the pressure, and u^ν the fluid four-velocity. The tensor $\eta^{\mu\nu}$ is the metric tensor describing the geometry of the fixed, flat space-time where the fluid evolves. In the following we will use $u^\mu = \gamma(1,\vec{v})$, γ being the Lorentz factor, $\gamma = 1/\sqrt{1-v^2}$.

The initial equilibrium configuration is that of a steady slab jet in Cartesian coordinates flowing along the z coordinate, surrounded by a denser and colder ambient medium. A single-component ideal gas equation of state with adiabatic exponent $\Gamma = 4/3$ has been used to describe both jet and ambient media. Both media are in pressure equilibrium and are separated by a smooth shear layer of the form [11]

$$a(x) = a_\infty + (a_0 - a_\infty)/\cosh(x^m), \tag{2}$$

where $a(x)$ is the profiled quantity (v_z and ρ the rest mass density) and a_0 and a_∞ its values at the jet symmetry plane (at $x=0$) and at $x \to \infty$, respectively. The integer m controls the shear layer steepness. In the limit $m \to \infty$ the configuration tends to the vortex-sheet case.

We now introduce an adiabatic perturbation of the form $\propto g(x)\exp[i(k_z z - \omega t)]$ in the flow equations, ω and k_z being the frequency and wave number of the perturbation along the jet flow. We shall follow the *temporal approach*, in which perturbations grow in time, having real wave numbers and complex frequencies (the imaginary part being the *growth rate*). The number of nodes across the planar jet, n_x, distinguishes between ordinary modes (corresponding to $n_x=0$) and reflection modes ($n_x>0$). By linearizing the equations and eliminating the perturbations of rest mass density and flow velocity, a second-order ordinary differential equation for the pressure perturbation P_1 is obtained [18]:

$$P_1'' + \left(\frac{2\gamma_0^2 v_{0z}'(k_z - \omega v_{0z})}{\omega - v_{0z}k_z} - \frac{\rho_{e,0}'}{\rho_{e,0} + P_0} \right) P_1' + \gamma_0^2 \left(\frac{(\omega - v_{0z}k_z)^2}{c_{s,0}^2} - (k_z - \omega v_{0z})^2 \right) P_1 = 0, \tag{3}$$

where $\rho_{e,0}$ is the energy density of the unperturbed model, P_0 the pressure, v_{0z} the three-velocity component, $\gamma_0 = 1/\sqrt{1-v_{0z}^2}$ the Lorentz factor, and $c_{s,0}$ the relativistic sound speed. The prime denotes the x derivative. Unlike the vortex-sheet case, in the case of a continuous velocity profile, a dispersion relation cannot be written explicitly. Equation (3) is integrated from the jet axis, where boundary conditions on the amplitude of pressure perturbation and its first derivative are imposed:

$$P_1(x=0) = 1, \quad P_1'(x=0) = 0 \text{(symmetric modes)},$$
$$P_1(x=0) = 0, \quad P_1'(x=0) = 1 \text{(antisymmetric modes)}. \tag{4}$$

Solutions satisfying the Sommerfeld radiation conditions (no incoming waves from infinity and wave amplitudes decaying towards infinity) are found with the aid of the method proposed in Ref. [19], based on the shooting method [20].

We have solved the linear problem for more than 20 models with different specific internal energies of the jet, Lorentz factors, and shear-layer widths, fixing the jet and ambient rest-mass density contrast (=0.1). We used $m=8, 25, 2000$ [shear layer width $d \approx (0.6, 0.177, 5\times10^{-3})R_j$] and vortex sheets for jets having specific internal energies $\varepsilon_j = 0.4c^2$ (models *B*) and $60c^2$ (models *D*) and Lorentz factors $\gamma_j = 5$ (*B*05, *D*05) and 20 (*B*20, *D*20). Solutions with $m=2000$ were considered in order to test the convergence to the vortex sheet in the case of narrow shear layers, with positive results. Also, fixing the width of the shear layer by setting $m=25$, we solved for $\varepsilon_j = 0.7c^2$ (model *A*), along with models *B* and *D*, using $\gamma_j = 2.5$ and 10, in order to span a wide range of parameters [21].

The effect of the shear layer on the linear stability is seen in Fig. 1 where we show the growth rates of the fundamental and a series of reflecting (antisymmetric) modes resulting from the solution of Eq. (3) together with the boundary conditions (4) for model *D*20. The corresponding solution for the vortex-sheet case is also shown for comparison.

We note that the reflection-mode solutions of the shear problem are more stable (i.e., the growth rates are smaller) for most wave numbers, especially in the large-wave-number limit, than the corresponding solutions in the vortex-sheet case. This behavior was reported for the first time for the first- and second-reflection modes in the nonrelativistic limit [11]. The growth rate curves corresponding to a single nth reflection mode consist of a broad maximum at larger wave numbers and a local peak which is placed in the small-wave-number limit, near the marginal stability point of the mode. While in the relativistic-jet, vortex-sheet case the small-wave-number peaks are relatively unimportant (since the

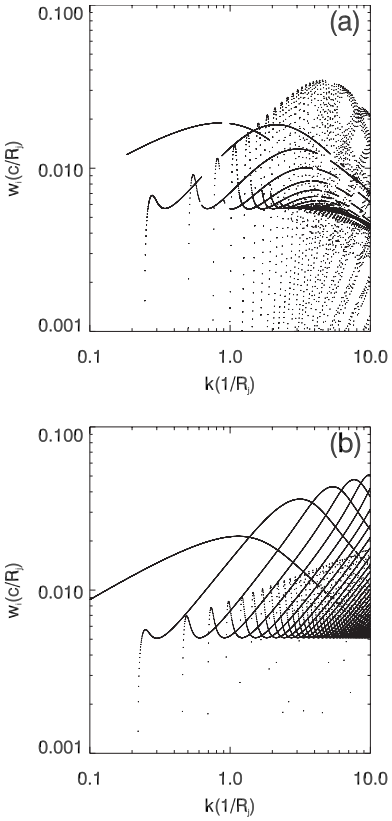

FIG. 1. Growth rate vs longitudinal wave number for model $D20$, using a shear layer with $m=25$ in Eq. (2) [panel (a)] and vortex sheet [panel (b)] for the fundamental and a series of reflection, antisymmetric modes including the one with the absolute maximum in the growth rate. The main differences are the overall decrease of growth rates in the sheared case and the appearance in this case of sharp resonances at the small-wave-number limit for each high-order reflection mode with the largest growth rates for a given mode.

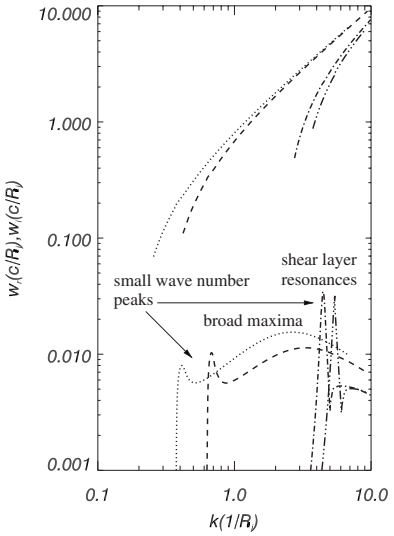

FIG. 2. Specific symmetric modes of model $D20$. Dotted line: first reflection mode. Dashed line: second reflection mode. Dash-dotted line: 20th reflection mode. Dash-triple dotted line: 25th reflection mode. We point out both the broad maxima and the small-wave-number peaks present in every single mode. Small-wave-number peaks of high-order reflection modes show larger growth rates and thus are defined as (shear-layer) resonances.

maximum growth rates at these peaks are lower than the growth rates of other unstable modes), in the presence of the shear layer they significantly dominate over other modes. Therefore we shall call these peaks the *shear-layer resonances* [22]. In Fig. 2 we show the solution for four specific symmetric modes (two low-order and two high-order reflection modes) of model $D20$. Low-order modes do not show strong peaks at maximum unstable wavelengths, whereas high-order reflection modes show peaks (the so-called shear-layer resonances) at this maximum wavelength and do not present broad maxima. The dependence of the properties of the growth rates associated with the shear-layer resonances on the jet-specific internal energy, jet Lorentz factor, and shear-layer parameter m can be summarized as follows: (i) An increase of the jet Lorentz factor enhances the dominance of resonant modes with respect to ordinary and low-order reflection modes; (ii) a decrease in the specific internal energy of the jet causes resonances to appear at longer wavelengths; (iii) a widening of the shear layer reduces the growth rates and the dominance of the shear-layer resonances, suggesting that there is an optimal width of the shear layer that maximizes the effect, for a given set of jet parameters; (iv) as the shear layer widens, the largest growth rate of resonant modes moves towards smaller wave numbers and lower-order reflection modes; (v) modes with wave number larger than some limiting value that decreases with the shear-layer width are damped significantly, consistent with previous nonrelativistic results [11].

The shear-layer resonances correspond to very distinct spatial structures of eigenmodes. In Fig. 3, we show maps of different structures generated in a jet by pressure perturbation, depending on the excited KH mode, as derived by theory and simulations. The structure of maximally unstable eigenmodes in the vortex-sheet case and nonresonant modes in the sheared case (upper panel of Fig. 3) represents a superposition of oblique sound waves in both the jet interior and the ambient medium. Contrarily, in the shear-layer case (central panel of Fig. 3), the most unstable resonant modes have a very large transversal wave number (the transversal wavelength is comparable to the width of the shear layer) in the jet interior and they are strongly damped in amplitude in the ambient medium. In order to demonstrate the relevance of the resonant modes in the evolution of the flow, we display in the bottom panel of Fig. 3 an analogous pressure map resulting from a numerical hydrodynamical simulation [23]. In this simulation an equilibrium jet corresponding to model $D20$ with $m=25$ (the value of m is 25 for all numerical simulations presented here, unless explicitly indicated) has been perturbed with a superposition of small-amplitude sinusoidal perturbations. The pressure snapshot displayed in the right panel of Fig. 3 corresponds to an early stage of the evolution in which the perturbation is still small (linear phase). The resonant mode starts to dominate in the numerical simulation due to its large growth rate, and its spatial structure is very similar to that of the most unstable (resonant) eigenmode obtained from the corresponding linear problem (central panel of Fig. 3).

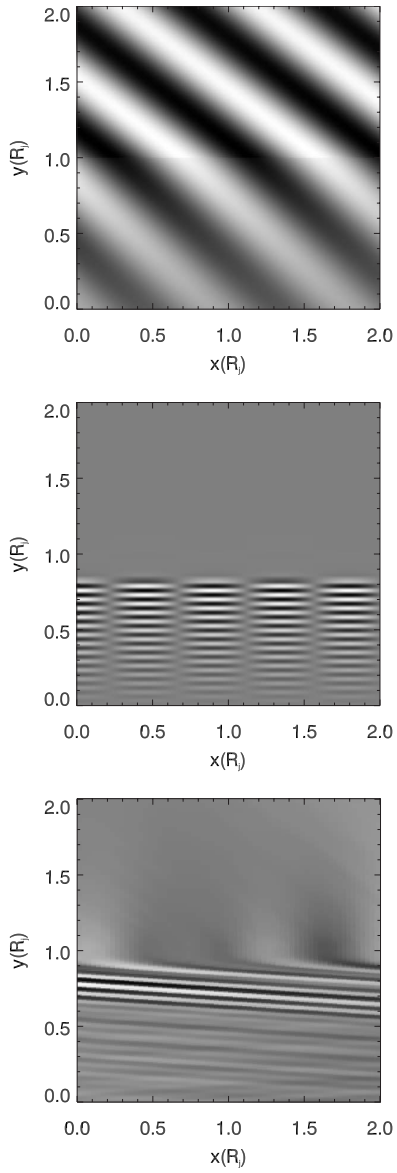

FIG. 3. Two-dimensional panels of different pressure perturbation structures for model $D20$. The gray scale extends over the pressure variations (in arbitrary units). Lengths are measured in (initial) jet radii R_j. Flow is from left to right and periodical. The bottom boundary corresponds to the jet symmetry plane. Top panel: vortex-sheet dominant mode (low-order reflection mode) at a given wavelength (from linear solution). Central panel: dominant mode (high-order reflection mode) at the same wavelength when $m=25$ [Eq. (2)] shear layer is included (also from a linear solution). Bottom panel: pressure perturbation map from a hydrodynamical simulation in the linear regime. The resolution used in the simulation was 256 cells/R_j across the jet and 32 cells/R_j, along. Grid size was $6R_j$ transversally and $8R_j$ axially, with an extended, decreasing resolution, grid in the transversal direction up to $100R_j$. Periodic boundary conditions were applied at the left and right ends of the grid and outflow boundary conditions far from the jet in the transversal direction.

Figure 4 shows two radial plots of the pressure perturbation, corresponding to model $D20$ introduced in the previous paragraph, at two different times [panels (a) and (b)] during

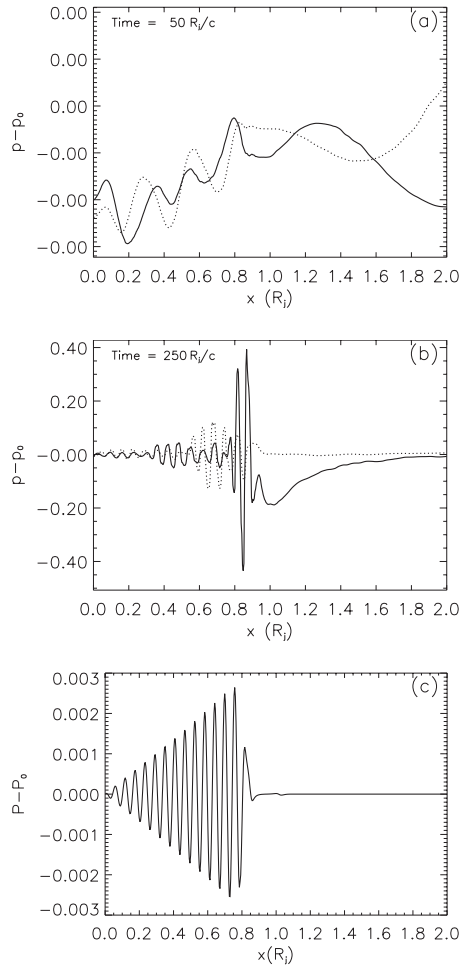

FIG. 4. Radial plots of pressure perturbation ($P-P_0$, with $P_0=2.0\rho_{\text{ext}}c^2$) at two different times in the simulation for model $D20$ (see the caption of Fig. 3 for details) and a theoretical representation of the transversal structure of the fastest-growing resonant mode, at the wavelength observed in the simulation, in arbitrary units [panel (c)]. The top panel (a) shows the perturbation in a moment when the resonant modes have not yet appeared, and the central panel (b) shows a moment when the resonant modes dominate the linear regime. The solid line stands for the pressure perturbation at $z=0R_j$, and the dotted line stands for the pressure perturbation at half grid $z=4R_j$.

the linear phase, before [panel (a)] and after [panel (b)] the resonant modes become dominant in the jet structure, emphasizing the conclusions derived from Fig. 3. A clear change in the transversal structure of the perturbation is observed, where the radial structure (small radial wavelength) of the growing resonant mode is displayed in the right panel (c) of Fig. 4. In Fig. 4(c), the theoretical profile of the fastest-growing resonant mode, at the wavelength found in the simulation, is shown. The number of zeros in the central and bottom panels is the same (29 in both cases), implying a correct identification of the mode (29th body mode). A difference in the amplitude profile of the mode is observed between this theoretical structure and that found in the simulations [Fig. 4(b)]. This is due to a growth of the modes faster than predicted by the theory in the shear layer, which might be caused by interactions between waves. The modulation of

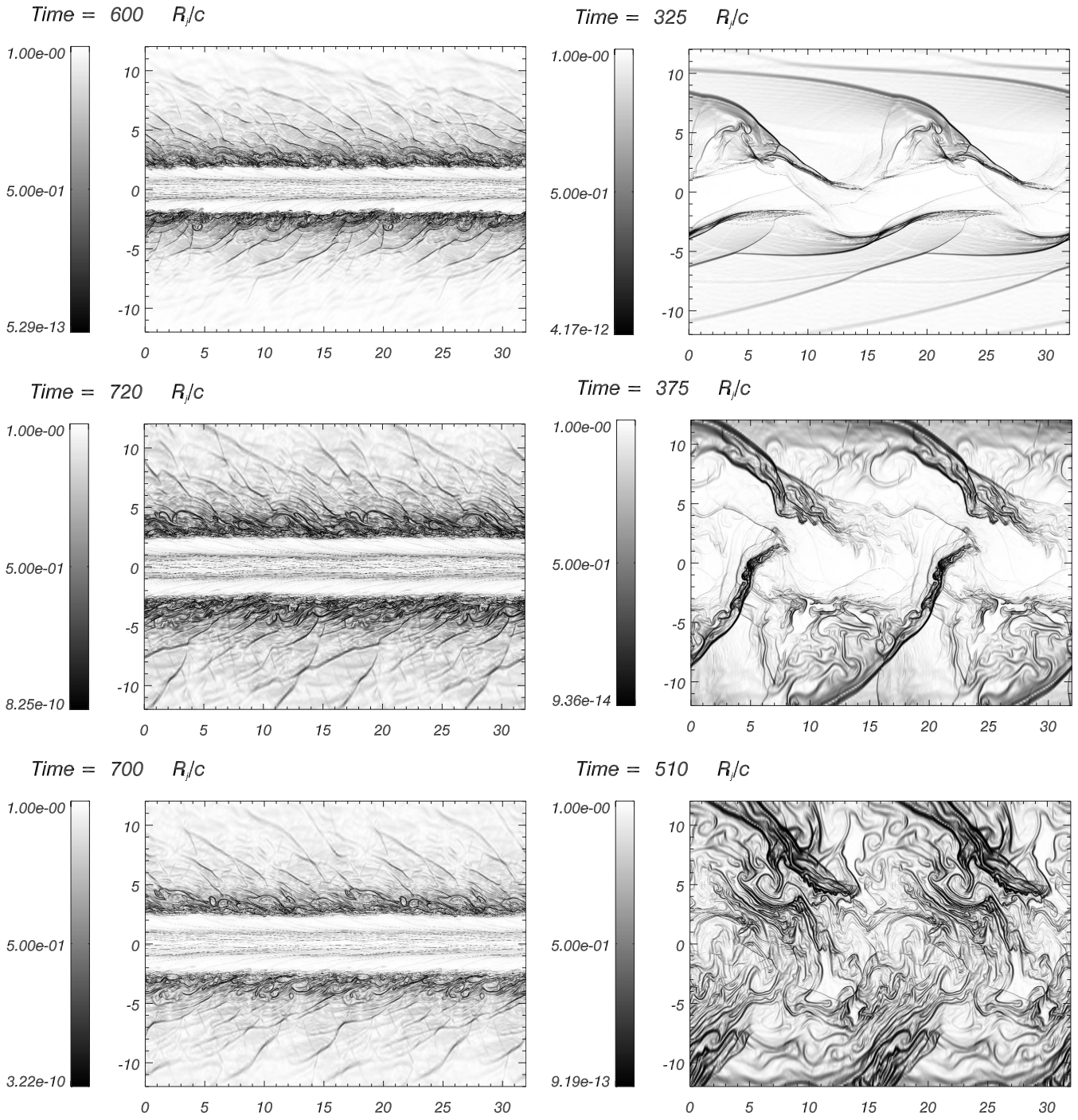

FIG. 5. Schlieren plots at different times in the nonlinear regime for models $B20$ (left panels), at times $t=(600,700,720)R_j/c$ and $B05$ (right panels) at times $t=(325,375,510)R_j/c$. Shear-layer resonances shield the jet in model $B20$ against disruption. Grid size was $6R_j$ transversally and $16R_j$ axially in these simulations (see the caption of Fig. 3 for further details).

amplitudes observed in Fig. 4(b) for radii $r<0.8R_j$ gives support to the idea of interference between modes.

III. NONLINEAR EVOLUTION

The importance of the shear-layer resonant modes relies not only on their dominance among solutions of the linearized problem. The numerical simulations show that whenever these modes appear (mostly in models with both high Lorentz factor and high relativistic Mach number) the transition of the overall perturbed jet structure to the nonlinear regime is significantly altered. In Fig. 5 we show how the resonant modes affect the nonlinear evolution of instabilities in jets with larger Lorentz factors and relativistic Mach numbers. The maps represent schlieren plots for model $B20$ ($\gamma=20$, left panels) and model $B05$ ($\gamma=5$, right panels). Model $B20$ shows a well-collimated jet with only small-scale variations in time, due to the development of resonant modes,

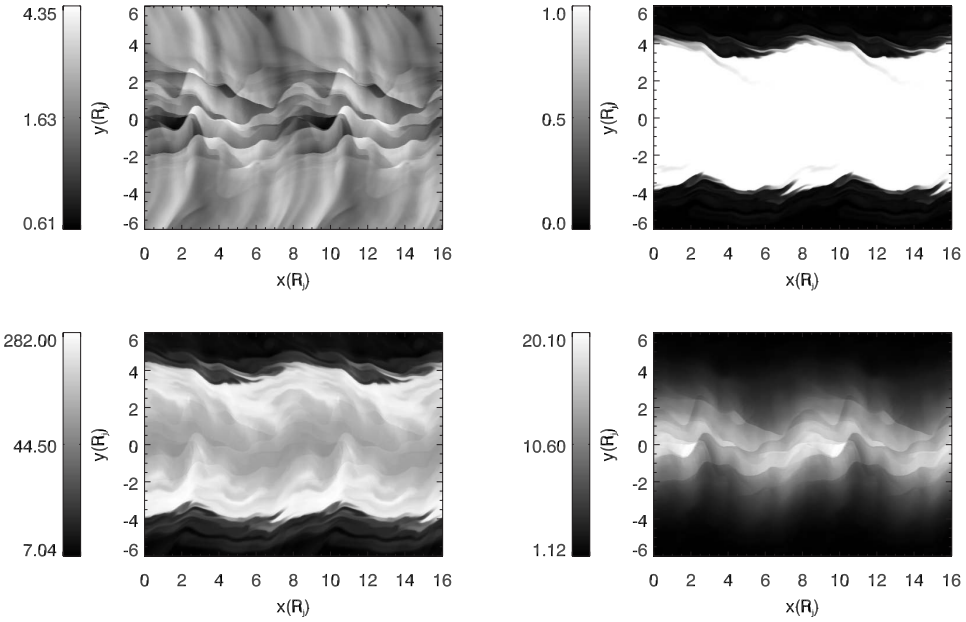

FIG. 6. Two-dimensional panels of the logarithm of pressure (top left), tracer (top right), logarithm of specific internal energy (bottom left), and Lorentz factor (bottom right) of model $D20$ at $t=1000R_j/c$, well inside the nonlinear regime and once an asymptotic quasisteady state has been reached. Lengths are measured in (initial) jet radii R_j. Initial tracer values are 1.0 for pure jet matter and 0.0 for pure ambient matter. As seen in the tracer panel, the final width of the jet is 3 times the initial one. A thick shear layer with high specific internal energy is observed in the bottom left panel.

whereas the jet in model $B05$ undergoes strong sideways oscillations which lead to the formation of strong oblique shocks (first panel) and the subsequent jet disruption.

By analyzing the long-term simulation results we find that those jets for which the resonant modes start to dominate early in the simulation do not disrupt, but instead widen and develop a thick long-standing layer of very large specific internal energy. An example of this behavior is shown in Fig. 6 where we show panels corresponding to the pressure, jet mass fraction (tracer), specific internal energy, and flow Lorentz factor for model $D20$ once an asymptotic quasisteady state has been reached. For comparison, Fig. 7 shows the equivalent set of panels to those in Fig. 6 for the vortex-sheet approximation case ($m=50$). Morphological and quantitative differences, as entrainment and jet disruption, are clearly observed. We thus find that these resonant modes shield jets against disruption. The presence of the hot boundary layer as well as the shear-layer resonant modes characterized by short radial wavelengths modify the interaction of the long-wavelength sound waves with the jet boundaries. Other facts pointing towards the nonlinear stabilizing role of the shear layer resonant modes are shown in Fig. 8, where the evolution of the normalized total longitudinal momentum and the width of the mixing layer are shown as a function of time. At the end of the simulation (at time $t=1000R_j/c$, well inside the nonlinear regime) model $D20$, with $m=25$, has transferred less than 4% of the axial momentum to the ambient medium, while in the corresponding vortex-sheet case it has transferred as much as 40% of the axial momentum at time $t=595R_j/c$ (see Figs. 6 and 7). The width of the mixing layer developed by this model in both the vortex-sheet limit and sheared-flow cases also points to the stabilizing role of the

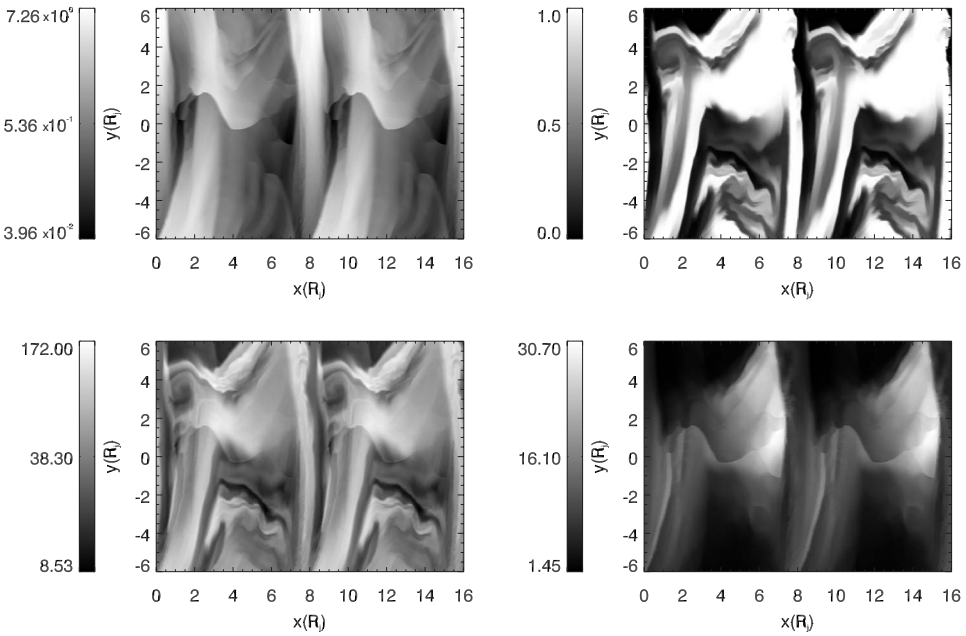

FIG. 7. Two-dimensional panels of the pressure (top left), tracer (top right), logarithm of specific internal energy (bottom left), and Lorentz factor (bottom right) of model $D20$, in the vortex-sheet analytical limit, at $t=595R_j/c$. Compare with Fig. 6.

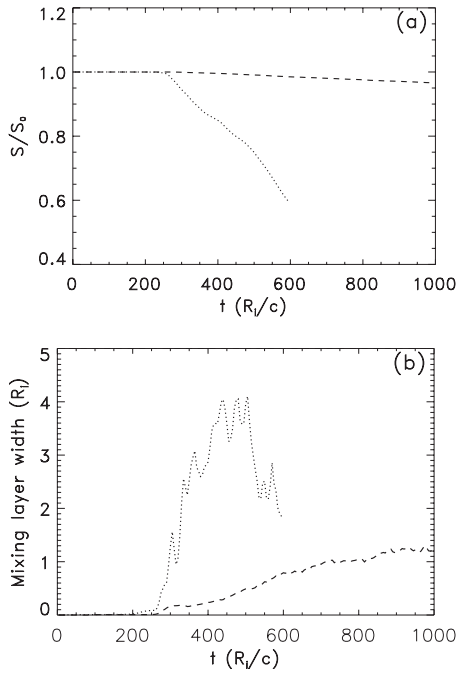

FIG. 8. Top panel (a) shows the evolution of the total longitudinal momentum, normalized to the initial value of the simulation, as a function of time, for the vortex-sheet analytical limit simulation (dotted line) and for the sheared-jet simulation (dashed line). The bottom panel (b) shows the width of the mixing layer, measured as the radial distance between tracer values of 0.95 and 0.05. The lines represent the same models as in panel (a).

shear-layer resonant modes. Whereas in the vortex case the mixing layer grows radially up to $4R_j$ with an expansion velocity $\sim 0.01c$, in the sheared case it only develops up to $1.2R_j$ and with a much smaller expansion velocity $\sim 1.2 \times 10^{-3}c$. The width of the mixing layer is computed as the distance between the outermost radius where the tracer (jet mass fraction) value is 0.95 and the innermost radius where its value is 0.05. Thus, the fall in the width of the mixing layer for the vortex case (dotted line in the plot) at the latest times of the simulation $[t=(500-600)R_j/c]$ is not due to a real reduction of this width, but to the fact that there are portions of pure jet material (where the tracer value is 1) moving at large radii and close to regions of the grid where the external medium material prevails (tracer ≈ 0), as can be seen in Fig. 7. This is just an artifact of the way in which the width of the mixing layer is computed.

IV. DISCUSSION

A. Nature of resonant modes

We have analyzed under general conditions the effect of shear on the stability properties of relativistic flows. The linear analysis has allowed us to discover resonant modes specific to the relativistic shear layer that have the largest growth rates. These modes are found to develop in high Lorentz factor and relativistic Mach number jets. The effects of the growth of these modes in the nonlinear stability of relativistic flows have been probed by a series of high-resolution hydrodynamical simulations.

Fourier analysis of the results of the numerical simulation shows that the fastest-growing mode corresponds to the one expected from the linear analysis. The growth rates found in the simulations are of the order of those predicted by linear theory close to the jet axis, but larger by factors ranging from 1.4 to 2.0 in the shear layer, depending on the jet parameters, than those predicted by the solutions to the linear stability problem, which might be due to nonlinear interactions between the perturbation waves in the shear layer.

Urpin [14] has studied the growth of instabilities in sheared jets. In [14] an analytical approach was done for the case of cold fluid jets with a velocity shear. One of the most important conclusions derived from that work is that the shear-layer instabilities found may grow faster than the KH instabilities in the vortex-sheet approximation (this fact was first pointed out by [12]). The similarities between the instabilities reported in this paper and those studied by Urpin [14] are found to be that (i) the growth rates are larger for hotter jets, (ii) the growth rates decrease for faster jets, and (iii) these instabilities are dominant for higher order modes. The resonant modes reported in this paper represent a manifestation of the so-called shear-driven instabilities, which were also reported by Urpin [14] for a specific set of physical conditions in the jet. However, the work reported in the present paper includes a wider set of jet parameters and support of the results of numerical simulations and solutions (found via numerical methods) of the differential equation of pressure perturbation. The latter permits a deeper analysis of the linear phase of growth of the instabilities. Also, the method developed in this paper is valid for any shape of the shear layer.

B. Formation of hot layers

The formation of a hot boundary layer surrounding the inner core of the jet as a consequence of the growth of resonant modes has been reported in the previous section on the nonlinear regime. In this section, the formation of such hot boundaries is explained.

The parallel and perpendicular wavelengths of the shear-layer resonant modes, λ_z and λ_x, respectively, are both small ($\lesssim R_j$) with $\lambda_x \ll \lambda_z$. Therefore their wave vectors are almost perpendicular to the jet axis, and thus the waves propagate from the shear layer towards the jet axis. On the other hand, the resonant modes have large growth rates, exceeding the growth rate of other modes, so they start to dominate the evolution. In [21] it was shown that the growth of instabilities goes through three main stages: linear phase, saturation phase, and nonlinear phase. The saturation of the linear growth of KH instabilities in relativistic flows is stopped when the amplitude of the velocity perturbation reaches the speed of light in the jet reference frame. As the maximum amplitude is reached, the sound waves propagating towards the jet axis (in the jet reference frame) steepen and form shock fronts. The fluid particles moving outwards from the jet interior cross the shock, decelerate, and increase their internal energy. In addition, turbulent motions of particles, as they go through shocks and generate small-scale velocity variations, also contribute to the conversion of kinetic energy

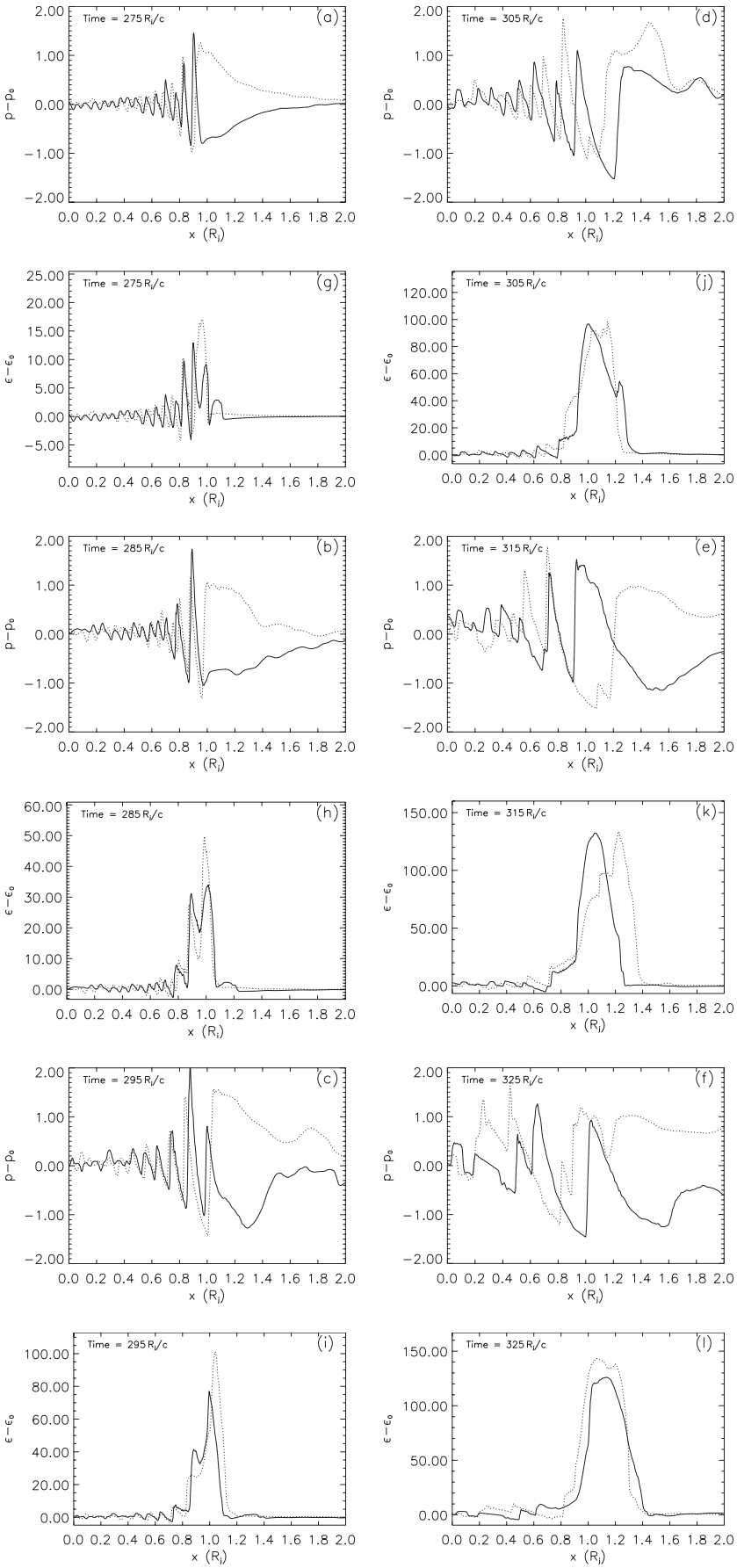

FIG. 9. Radial plots of pressure perturbation $[P-P_0$, with $P_0=2.0\rho_{ext}c^2$, panels (a)–(f)] and specific internal energy $[\varepsilon-\varepsilon_0$, with $\varepsilon_0=60.0c^2$, panels (g)–(l)] at different times in simulation of model *D*20. The solid line stands for the pressure perturbation at $z=0R_j$, and the dotted line stands for the pressure perturbation at half grid $z=4R_j$. The plots show how the steepening of the pressure waves and dissipation in shocks leads to heating of the shear layer. Note the different scales (increase of the maxima with time) for the specific internal energy perturbation plots.

into internal energy. Figure 9 illustrates the process of generation of the hot shear layer which protects the central core of the jet at the end of the linear regime for model $D20$. In the left panels [panels (a)–(f)] we display radial plots of the pressure perturbation at different times in the transition from the linear to the nonlinear regime. The plots show how the maxima of the pressure perturbation appear in the shear layer and how the waves steepen. In the right panels [(g)–(l)] we display radial plots of the perturbation in specific internal energy and show how the shocks produced by the steepening of the waves expand and heat the shocked material in the shear layer.

V. IMPLICATIONS FOR EXTRAGALACTIC JETS

Our results offer an explanation to the morphological FRI-FRII dichotomy of large-scale extragalactic radio jets [24] and its present paradigm. This dichotomy consists of a morphological classification of extragalactic jets, being FRII sources those showing a high collimation and bright hot spot at the point of collision with the ambient and FRI sources those showing a diffuse and decollimated morphology in their outer regions. The latter have been interpreted as due to jet disruption and mass loading of the original flow [25]. The growth of the shear-layer resonances in the highly relativistic models considered in this paper can explain the remarkable collimation and stability properties of powerful radio jets. Current theoretical models [25] interpret FRI morphologies as the result of a smooth deceleration from relativistic ($\gamma \leqslant 3$ [26]) to nonrelativistic transonic speeds ($\sim 0.1c$) on kpc scales. On the contrary, radio-flux asymmetries between jets and counterjets in the most powerful radio galaxies and quasars (FRII) indicate that relativistic motion ($\gamma \sim 2-4$ [27]) extends up to kpc scales in these sources. In addition, current models for high-energy emission from powerful jets at kpc scales [28] offer additional support to the hypothesis of relativistic bulk speeds on these scales. This whole picture is in agreement with the results presented here as the development of resonant, stabilizing modes occurs in faster jets, while slower jets appear to be disrupted by entrainment of ambient material and slowed down to $v < 0.5c$ during their evolution. These conclusions point to an important contribution by intrinsic properties of the source to the morphological dichotomy. Nevertheless, the importance of the ambient medium cannot be ruled out on the basis of our simulations, since we consider an infinite jet in pressure equilibrium flowing in an already open funnel and surrounded by a homogeneous ambient medium.

There are plenty of arguments indicating the existence of transversal structure in extragalactic jets at all scales [9,17,29]. We have found the development of relatively thin ($\approx 2R_j$), hot shear layers in models affected by the growth of resonant modes to nonlinear amplitudes, as discussed in this paper. These hot shear layers could explain several observational trends in the transversal structure of powerful jets at both parsec and kiloparsec scales [29]. Conversely and according to our simulations, these transition layers could be responsible for the stability of fast, highly supersonic jets, preventing the mass loading and subsequent disruption. Thicker, mixing layers formed in slower jets could mimic the transition layers invoked in models of FRIs [25].

Direct comparison of our results with real jets is, however, still difficult due to the slab geometry of the problem studied here and to the fact that magnetic fields are not considered in our work. The latter are known to be present in extragalactic jets and even to be dynamically important for the evolution of compact jets. Several authors have studied their influence on the stability these objects [30]. The inclusion of magnetic fields and three-dimensional cylindrical geometries in linear calculations and numerical simulations is a natural further step in our work.

ACKNOWLEDGMENTS

Calculations were performed on the SGI Altix 3000 computer CERCA at the Servei d'Informàtica de la Universitat de València. This work was supported by the Spanish DGES under Grant No. AYA-2001-3490-C02 and Conselleria d'Empresa, Universitat i Ciencia de la Generalitat Valenciana under Project No. GV2005/244. M.P. benefited from support from the Universitat de València (V Segles program) and the Max-Planck-Institut für Radioastronomie in Bonn.

[1] S. Chandrasekhar, *Hydrodynamic and Hydromagnetic Stability* (Clarendon Press, Oxford, 1961); A. E. Gill, Phys. Fluids **8**, 1428 (1965); R. A. Gerwin, Rev. Mod. Phys. **40**, 652 (1968).
[2] B. D. Turland and P. A. G. Scheuer, Mon. Not. R. Astron. Soc. **176**, 421 (1976); R. D. Blandford and J. E. Pringle, *ibid.* **176**, 443 (1976).
[3] A. Ferrari *et al.*, Astron. Astrophys. **64**, 43 (1978).
[4] P. Hardee, Astrophys. J. **234**, 47 (1979).
[5] P. Hardee, Astrophys. J. **313**, 607 (1987).
[6] P. Hardee, Astrophys. J. **318**, 78 (1987).
[7] E.g., P. E. Hardee, Astrophys. J. **250**, 9 (1981); P. E. Hardee and M. L. Norman, *ibid.* **342**, 680 (1989); J.-H. Zhao *et al.*, *ibid.* **387**, 69 (1992).
[8] Pinching KH modes generate radio knots with distinct kinematical properties [I. Agudo *et al.*, Astrophys. J., Lett. Ed. **549**, 183 (2001)]; The instabilities forced by precession and wave-wave interactions can explain differentially moving features in the jets; [P. E. Hardee *et al.*, Astrophys. J. **555**, 744 (2001)]; It was possible to interprete the structure and motions of the 3C120 jet (0.6—300 pc) on the basis of KM instabilities [R. C. Walker *et al.*, *ibid.* **556**, 756 (2001)]; The internal structure and dynamics of the M87 jet were understood using the KH linear analysis [A. P. Lobanov *et al.*, New Astron. Rev. **47**, 629 (2003)].
[9] A. P. Lobanov and J. A. Zensus, Science **294**, 128 (2001).
[10] W. Blumen *et al.*, J. Fluid Mech. **71**, 305 (1975); P. G. Drazin and A. Davey, *ibid.* **82**, 255 (1977).
[11] A. Ferrari *et al.*, Mon. Not. R. Astron. Soc. **198**, 1065 (1982).

[12] M. Birkinshaw, Mon. Not. R. Astron. Soc. **252**, 505 (1991).
[13] M. Hanasz and H. Sol, Astron. Astrophys. **315**, 355 (1996).
[14] V. Urpin, Astron. Astrophys. **385**, 14 (2002).
[15] A. Rosen *et al.*, Astrophys. J. **516**, 729 (1999); P. E. Hardee, *ibid.* **533**, 176 (2000); P. E. Hardee *et al.*, *ibid.* **555**, 744 (2001).
[16] M. A. Aloy *et al.*, Astron. Astrophys. **396**, 693 (2002).
[17] M. Perucho, J. M. Martí, and M. Hanasz, Astron. Astrophys. **443**, 863 (2005).
[18] The equation was first derived by M. Birkinshaw, Mon. Not. R. Astron. Soc. **208**, 887 (1984).
[19] S. Roy Choudhury and R. V. E. Lovelace, Astrophys. J. **283**, 331 (1984).
[20] W. H. Press *et al.*, *Numerical Recipes* (Cambridge University Press, Cambridge, England, 1997).
[21] The notation for the models follows that of M. Perucho *et al.*, Astron. Astrophys. **427**, 415 (2004) and M. Perucho *et al.*, *ibid.* **427**, 431 (2004) where the linear and nonlinear stability of relativistic planar jets in the vortex-sheet case was investigated.
[22] Some resonances due to the presence of a shear layer [12] or a sheath surrounding relativistic jet component [13] could appear as oscillations (*ripples*) on the growth rate curve in the large-wave-number limit; however, we do not observe oscillations of this type in our case. These ripples could be related to the presence of discontinuities in the jet-ambient transition, to the shape of the shear layer, or associated with a different region in parameter space.
[23] Numerical simulations were performed using a finite-difference code based on a high-resolution shock-capturing scheme which solves the equations of relativistic hydrodynamics written in conservation form [J. M. Martí *et al.*, Astrophys. J. **479**, 151 (1997)]. The code was recently parallelized using open-message passing (OMP) directives.
[24] B. L. Fanaroff and J. M. Riley, Mon. Not. R. Astron. Soc. **167**, 31 (1974).
[25] R. A. Laing and A. H. Bridle, Mon. Not. R. Astron. Soc. **336**, 328 (2002); **336**, 1161 (2002).
[26] T. J. Pearson, in *Energy Transport in Radio Galaxies and Quasars*, edited by P. E. Hardee, A. H. Bridle, and J. A. Zensus (ASP Conference Series, San Francisco, 1996), p. 97.
[27] A. H. Bridle *et al.*, Astrophys. J. **108**, 766 (1994).
[28] A. Celotti and R. D. Blandford, in *Proceedings of Black Holes in Binaries and Galactic Nuclei*, edited by L. Kaper, E. P. J. van den Heuvel, and A. P. Woudt (Springer, Berlin, 2001), p. 206.
[29] M. R. Swain *et al.*, Astrophys. J. **508**, L29 (1998); J. M. Attridge *et al.*, Astrophys. J., Lett. Ed. **518**, 87 (1999).
[30] See P. E. Hardee, in *Relativistic Jets*, edited by P. A. Hughes and J. N. Bregman (AIP, Melville, NY, 2006), p. 57, and references therein.